The Crystal Structure, Mutagenesis, and Activity Studies Reveal that Patatin Is a Lipid Acyl Hydrolase with a Ser-Asp Catalytic Dyad‡

Timothy J. Rydel,*,§,|| Jennifer M. Williams,§ Elysia Krieger,§ Farhad Moshiri,§ William C. Stallings,⊥ Sherri M. Brown,§ Jay C. Pershing,§ John P. Purcell,§ and Murtaza F. Alibhai§,||

Monsanto Company, Chesterfield, Missouri 63017-1732, and Pharmacia Corporation, Chesterfield, Missouri 63017-1732

Received November 11, 2002; Revised Manuscript Received March 28, 2003

ABSTRACT: Patatin is a nonspecific lipid acyl hydrolase that accounts for approximately 40% of the total soluble protein in mature potato tubers, and it has potent insecticidal activity against the corn rootworm. We determined the X-ray crystal structure of a His-tagged variant of an isozyme of patatin, Pat17, to 2.2 Å resolution, employing SeMet multiwavelength anomalous dispersion (MAD) phasing methods. The patatin crystal structure has three molecules in the asymmetric unit, an *R*-factor of 22.0%, and an R_{free} of 27.2% (for 10% of the data not included in the refinement) and includes 498 water molecules. The structure notably revealed that patatin has a Ser-Asp catalytic dyad and an active site like that of human cytosolic phospholipase A_2 (cPLA$_2$) [Dessen, A., et al. (1999) *Cell 97*, 349−360]. In addition, patatin has a folding topology related to that of the catalytic domain of cPLA$_2$ and unlike the canonical α/β-hydrolase fold. The structure confirms our site-directed mutagenesis and bioactivity data that initially suggested patatin possessed a Ser-Asp catalytic dyad. Alanine-scanning mutagenesis revealed that Ser77 and Asp215 were critical for both esterase and bioactivity, consistent with prior work implicating a Ser residue [Strickland, J. H., et al. (1995) *Plant Physiol. 109*, 667−674] and a Ser-Asp dyad [Hirschberg, H. J. H. B., et al. (2001) *Eur. J. Biochem. 268*, 5037−5044] in patatin's catalytic activity. The crystal structure aids the understanding of other structure−function relationships in patatin. Patatin does not display interfacial activation, a hallmark feature of lipases, and this is likely due to the fact that it lacks a flexible lid that can shield the active site.

Patatin is a member of a family of proteins found in potato and other solanaceous plants (*1*, *2*). In potatoes, patatin is predominantly found in tubers and at much lower levels in other plant organs (*3*). Genes that encode patatins have been previously isolated and characterized (*4*−*6*). These proteins have been shown to have lipid acyl hydrolase activity, and catalyze the nonspecific hydrolysis of phospholipids, glycolipids, sulfolipids, and mono- and diacylglycerols (*7*−*11*). Potato tubers contain many isoforms of patatin whose sequences are homologous (85−98%) and are immunologically identical (*4*, *5*, *12*). Patatins can be N-glycosylated (*13*), and while the glycosylation does not affect its proteolytic or enzymatic properties (*14*), the molecule's charge hetereogeneity is likely impacted by its glycosylation pattern (*12*). In addition, patatin was shown to have insecticidal activity against corn rootworm, an economically destructive insect pest in corn (*9*).

Comparison of patatin with other lipases indicates that it has the conserved amino acid motif (Gly-X-Ser-X-Gly) characteristic of esterases (*4*−*6*, *10*). Chemical modification studies on patatin using diisopropyl fluorophosphate (DFP)[1] eliminate both the enzymatic and insecticidal activities (*9*). DFP preferentially and irreversibly reacts with active site Ser residues. On the basis of the chemical modification studies of Strickland et al., the Ser residue in the hydrolase motif Gly-X-Ser-X-Gly was hypothesized to be the active site residue in patatin (*9*). Since patatin possesses lipid acyl hydrolase activity and contains an active site Ser residue, a catalytic triad composed of Ser, His, and Asp or Glu might be proposed, as such catalytic triads are frequently observed in lipases (*15*). In a recent study (*16*), researchers surmised that patatin B2 may possess a Ser-Asp catalytic dyad, based on a promising partial sequence alignment of this patatin with human cytosolic phospholipase A_2 (cPLA$_2$), which is known to possess a Ser-Asp catalytic dyad (*17*), and verified that this was indeed likely through mutagenesis and enzymatic activity studies.

Patatin inhibits the growth of corn rootworm in a dose-dependent manner when it is fed to these insects on an artificial diet, and could be of potential use for corn rootworm control strategies (*9*). In an effort to clarify the residues and structural determinants critical to patatin's enzymatic and insecticidal activity, we determined its X-ray crystal structure, performed alanine-scanning mutagenesis (*18*, *19*), and conducted enzymatic and insecticidal activity assays on selected

‡ Coordinates have been deposited in the Protein Data Bank as entry 1OXW.

* To whom correspondence should be addressed: Monsanto, Mail Zone GG4D, 700 Chesterfield Parkway W., Chesterfield, MO 63017-1732. Telephone: (636) 737-5642. Fax: (636) 737-7015. E-mail: timothy.j.rydel@monsanto.com.

§ Monsanto Company.

|| These authors contributed equally to the success of this study.

⊥ Pharmacia Corporation.

[1] Abbreviations: Bt, *Bacillus thuringiensis*; DFP, diisopropyl fluorophosphate; SCRW, Southern corn rootworm; cPLA$_2$, cytosolic phospholipase A_2; PLA$_2$, phospholipase A_2.

10.1021/bi027156r CCC: $25.00
Published on Web 05/16/2003

variants. When this work was initiated, no known crystal structures of patatin homologues were known. Therefore, we chose to determine the structure via selenomethionine (SeMet) multiwavelength anomalous dispersion (MAD) methods, previously proven to expedite the structure determination of new protein structures (*20*). The enzyme construct for crystallography was an isozyme of patatin, Pat17, in which the 23-amino acid N-terminal signal sequence was replaced with a 10-amino acid hexahistidien tag. The construct was expressed in *Escherichia coli* and incorporated selenomethionine (SeMet) instead of Met. The 2.2 Å resolution X-ray crystal structure clearly revealed that patatin possessed a Ser-Asp catalytic dyad, Ser77-Asp215, and an active site similar to that observed in the catalytic domain of human cytosolic phospholipase A_2 (cPLA$_2$) (*17*). The patatin fold appears to be related to that adopted by the catalytic domain of cPLA$_2$ and distinct from that of the α/β-hydrolase fold family (*21*), a fold commonly observed in lipases. Finally, a defining characteristic of lipases is the phenomenon known as "interfacial activation" (*22*, *23*), the greatly enhanced enzymatic activity observed when a lipase cleaves substrates presented at a membrane interface. The patatin crystal structure provides insight into why this enzyme does not display interfacial activation (*24*).

Alanine-scanning mutagenesis was used to identify the likely catalytic residues of patatin Pat17 in this work. All the charged residues in Pat17 were mutated to alanines in groups of one to three residues. These variants were expressed in *Pichia pastoris* and assayed for enzyme activity. Variants with no detectable activity but normal expression (as assessed by immunoblotting and an ELISA) were subsequently purified, further characterized, and assayed for insecticidal activity. On the basis of the consensus esterase motif, Gly-X-Ser-X-Gly, the Ser77 residue was mutated to verify that this indeed is the Ser residue responsible for catalytic and insecticidal activity. The mutational, enzymatic, and insecticidal activity data indicate that residues Ser77 and Asp215 are critical for patatin's enzymatic and insecticidal activity, which is consistent with results observed by other researchers (*9*, *16*) and with the crystal structure. In addition, these studies identified a His residue, His109, as being important in maintaining enzyme stability. Examining the crystal structure provided insights into the importance of this His residue.

EXPERIMENTAL PROCEDURES

Pat17 Cloning. Genes for patatin have been cloned by several investigators (*4*). Conserved patatin sequences were used to design primers to clone several patatin genes from *Solanum cardiophyllum*. Total RNA was prepared from tubers using Tri Reagent according to the manufacturer's protocol (Molecular Research Center, Inc.). The RNA was used to generate cDNA by means of reverse transcriptase. The full-length cDNA of one of the cloned isozymes, Pat17, was re-amplified by PCR using the primers 5′-GTTAGATCTCA*CCATGG*CAACTACTAAATCTTT-3′ (*Nco*I site in italics) and 5′-CCA*GAATTC*TCATTAATAAGAAGCTTTGTTTGC-3′ (*Eco*RI site in italics) using standard PCR conditions as described in the Gene Amp kit (Perkin-Elmer Cetus) and an annealing temperature of 40 °C. Resulting DNA was cloned into pBluescript (Stratagene) and sequenced. The final clone was named pMON26820. The Pat17 nucleotide sequence from *S. cardiophyllum* was deposited in GenBank as entry AY033231.

Expression and Purification of Selenomethionine-Containing Patatin from E. coli. The patatin construct used for crystallography had the initial 23-amino acid Pat17 signal sequence replaced with the 10-amino acid hexahistidine tag (MHHHHHHAMA). The convention used for numbering the patatin residues in the crystallography construct maintains the full Pat17 sequence numbering so that the crystallography construct extends from residue Met14 to Tyr387. Pat17 was expressed in *E. coli* using the pET expression system (Novagen, Madison, WI). The coding region of the mature Pat17 gene (without its signal peptide) was amplified by PCR with the primers 5′-GGG*CCATGG*CGCAGTTGGGAGAAATGGTG-3′ (*Nco*I site in italics) and 5′-AACAAAGCTTCTTATTGAGGT*GCGGCCGC*TTGCATGC-3′ (*Not*I site in italics) under standard PCR conditions, and by using plasmid pMON26820 as the template. The resulting DNA was digested with *Nco*I and *Not*I and cloned into a modified pET24d plasmid, designed to add an N-terminal hexahistidine tag to the protein. The correct sequence of the PCR product was verified by sequencing; the plasmid was transformed into the methionine auxotrophic *E. coli* strain B834(DE3) (Novagen), and transformants were selected on Luria Bertani (LB) plates containing 25 mg/L kanamycin. Growth in M9 minimal medium supplemented with 40 mg/L L-selenomethionine (Sigma, St. Louis, MO) was carried out according to published procedures (*25*). After induction for 8 h at 28 °C with 1 mM IPTG, cells were harvested and washed in 50 mM Tris-HCl (pH 8.5) and 150 mM NaCl and lysed with a French press at 20 000 psi. The His-tagged protein was recovered in the soluble fraction of the cell lysate and subsequently purified by chromatography on a Ni−NTA column as described by the manufacturer (Qiagen). The partially purified protein was dialyzed against 25 mM Tris-HCl (pH 7.5) and purified to homogeneity by chromatography on a Mono Q HR 10/10 column, exactly as described below for the *P. pastoris*-expressed protein, without the second Phenyl Sepharose chromatography step. The protein-containing fractions were pooled, concentrated, dialyzed against 25 mM Tris-HCl (pH 7.5), and stored at 4 °C.

Crystallization, Data Collection, and Data Processing. The Pat17 enzyme was crystallized using the technique of vapor diffusion by hanging drops. The protein sample was at a concentration of 10 mg/mL in 10 mM Tris buffer (pH 7.4), and the precipitant solution was 16% PEG 3350 and 0.24 M ammonium acetate. A droplet comprising 2 μL of protein solution and 2 μL of precipitant solution was placed on a siliconized coverslip and suspended over a grease-sealed well of a Linbro plate containing 500 μL of precipitant solution. Crystals appeared within 5 days. Preliminary in-house diffraction analyses on cryocooled crystals were conducted using a Molecular Structure Corp. (MSC) R-AXIS IV imaging plate detector mounted on an MSC RU300H3R X-ray generator, operating at a power of 50 kV and 100 mA, with beam collimation provided by MSC/Yale mirrors. Cryocooling was achieved using an MSC X-Stream unit operating at approximately −140 °C. Crystals taken from the drops were dipped in a cryosolution which was 16.5% PEG 3350, 0.23 M ammonium acetate, and 25% ethylene glycol prior to being flash-cooled in the cold stream of the R-AXIS IV unit. Use of the macromolecular crystal anneal-

ing method eliminated the problematic mosaicity in the patatin crystals and resulted in high-quality, single-lattice X-ray diffraction (*26*). Data analysis revealed that the crystals were in space group $C222_1$, diffracted to at least 2.5 Å resolution, and had the following unit cell dimensions: $a =$ 97.2 Å, $b =$ 171.4 Å, and $c =$ 129.8 Å. Assuming three patatin molecules per asymmetric unit results in a Matthews parameter (*27*) of 2.16 Å^3/Da and a solvent content of 43%, which is reasonable and consistent with the high-quality diffraction displayed by this crystal form.

Complete phasing by the molecular replacement method (*28*) was never considered as an option in the patatin structure determination. At the time this work was initiated, no crystallographic coordinates for any known structural homologues of patatin were available. The structure was determined using the *de novo* SeMet multiwavelength anomalous dispersion (MAD) phasing method. Four wavelengths of MAD data ($\lambda_1 =$ 0.9791 Å, $\lambda_2 =$ 0.9792 Å, $\lambda_3 =$ 1.019 Å, and $\lambda_4 =$ 0.942 Å) were collected at the IMCA 17-ID beamline of the APS synchrotron. A Marresearch CCD detector was used to collect the diffraction data. This data collection crystal, which was transferred to the synchrotron in a cryo-dewar, had previously been treated using the macromolecular crystal annealing method and its high-quality diffraction validated using an R-AXIS IV detector system. Three hundred sixty degrees of data at each wavelength were collected using 2.5 s exposures, an oscillation angle of 0.5°, and a crystal−detector distance of 130 mm. The data were reduced using the HKL2000 package (*29*).

Structure Determination and Refinement. SOLVE version 1.15 (*30*) was employed to locate the Se sites in the asymmetric unit and calculate phases using the 20−2.2 Å MAD data. SOLVE calculations were performed using unmerged, HKL2000-processed data from all four wavelengths and over the resolution ranges of 20−2.2 and 20−2.5 Å. Phases from SOLVE were improved using the CCP4 package (*31*) utility DM. Examination of a resulting 20−2.2 Å electron density map using an SGI Octane workstation with stereographics capability and the program O (*32*) clearly revealed that there were three molecules in the asymmetric unit. A single patatin Pat17 molecule was built into the map using the program O and the InsightII Biopolymer module (Accelrys, Inc.). The single-molecule Pat17 coordinates, 8−3.5 Å data measured a λ_4 of 0.942 Å in the MAD experiment, and the AMoRe molecular replacement package (*33*) were used to locate the remaining two molecules in the asymmetric unit.

Eight rounds of iterative crystallographic refinement with X-PLOR98 (*34*) and map fitting with the program O were then conducted to improve the structure. Data over the resolution range of 20−2.2 Å for which $F \geq 2\sigma(F)$ were used in the refinement; a bulk solvent mask correction was employed, with 10% of the data used to calculate the R_{free} (*35*) and 90% of the data used to calculate a conventional *R*-factor, R_{work}. Noncrystallographic symmetry (NCS) restraints were used in the refinement from the beginning. NCS-related atoms were restrained in their average positions using "group" equivalent atom statements and appropriate weights. Maximum likelihood refinement (*36*) protocols were used in the later stages. The refinement progress was evaluated by improvement in the quality of the electron density maps, by reduced values of R_{work} and R_{free}, and by evaluation of the coordinates produced through refinement with PROCHECK (*37*). Electron density maps employing the coefficients $2|F_o| - |F_c|$ and $|F_o| - |F_c|$ were examined simultaneously during the map examination and model modification work. Solvent molecules were added prior to the third round of refinement and thereafter, when appropriate. Peaks in the $|F_o| - |F_c|$ difference map satisfying a $\geq 2.5\sigma$ cutoff level and distance constraints to polar atoms in the structure were selected as water molecules.

Site-Directed Mutagenesis. Pat17 variants were generated using the oligonucleotide-directed mutagenesis protocol from Bio-Rad Laboratories (Richmond, CA), which is based on the method of Kunkel (*38*). Single-stranded DNA from pMON26820 was the template used for mutagenesis. Mutagenic oligonucleotides were purchased from Midland Reagent Co. (Midland, TX). Mutant clones were confirmed by sequencing.

Protein Expression in P. pastoris. Wild-type Pat17 and the generated variants were subcloned as *Xho*I−*Eco*RI fragments into the respective sites in the *P. pastoris* expression vector pPIC9 (Invitrogen). These constructs were used for the secretion and extracellular expression of the proteins. The transformation of the *P. pastoris* strain KM71 (Invitrogen), screening for recombinants, and expression experiments were performed as outlined in the instruction manual.

Enzyme Activity Assays, Immunoblotting, and an ELISA. Enzyme activity was measured as described previously using *p*-nitrophenyl caprate or *p*-nitrophenyl octanoate (Sigma) as the substrate (*3*). Stock solutions (5 mM) of the substrate in dimethyl sulfoxide were diluted in 4% Triton X-100 and 1% SDS to a final concentration of 1 mM. For the standard assay, 25 μL of the 1 mM substrate solution was added to 80 μL of 50 mM Tris-HCl (pH 8.5) prior to the addition of 20 μL of protein solution (final substrate concentration of 0.2 mM). The optical density was monitored at 405 nm in 6 s intervals for a period of 10 min. Esterase activity of the variants was normalized to that of the wild-type enzyme and expressed as the ratio of the activities using *p*-nitrophenyl octanoate and *p*-nitrophenyl caprate as substrates. Enzyme assay data for purified enzymes were calculated as specific activities, based on the Bradford protein assay (Bio-Rad), using bovine serum albumin as a standard. Immunoblotting and an ELISA were performed on all variants to estimate qualitative yield and to confirm electrophoretic mobility equivalent to that of wild-type Pat17. The ELISA was performed using monoclonal antibody B4A1 (Monsanto Co.) as the capture agent and rabbit anti-patatin polyclonal antibody (P3752) as the detecting antibody. Immunodetection on Western blots was done using the P3752 polyclonal antibody/anti-rabbit HRP-conjugated antibody and the ECL detection system (Amersham Pharmacia Biotech, Piscataway, NJ).

Enzyme Purification and Steady-State Kinetic Assays. Culture supernatants of *P. pastoris* clones producing recombinant protein were concentrated and dialyzed against 25 mM Tris-HCl at pH 7.5 (buffer A) and loaded onto a Mono Q HR 10/10 anion-exchange column (Amersham Pharmacia Biotech) equilibrated with buffer A. The protein was eluted with a linear gradient from 0 to 1 M KCl in buffer A, run over 30 min at a flow rate of 4 mL/min using an HPLC system (Shimadzu). Fractions containing protein based on the absorbance at 280 nm were analyzed by SDS−PAGE

Table 1: Data Collection, Phase Determination, and Refinement Statistics

	Data Collection			
	peak	inflection	remote 1	remote 2
space group	$C222_1$			
unit cell	$a = 97.2$ Å, $b = 171.4$ Å, $c = 129.9$ Å, $\alpha = \beta = \gamma = 90°$			
wavelength (Å)	0.9791	0.9792	1.019	0.9419
maximum resolution (Å)	2.2	2.2	2.2	2.2
R_{sym} (%)[a]	7.7 (21.8)	9.2 (21.0)	7.1 (16.8)	8.6 (27.3)
completeness (%)	100.0	100.0	99.8	100.0
total no. of reflections	762165	784440	804317	793816
no. of unique reflections[b]	55261	55074	55251	55374
average multiplicity	13.8	14.2	14.6	14.3
$\langle I/\sigma(I)\rangle$	37.2 (7.3)	33.2 (7.1)	44.5 (13.5)	36.2 (7.0)
f'(e−)	−7.50	−10.28	−2.9	−1.9
f''(e−)	5.94	3.40	0.4	3.1

MAD Phasing with SOLVE

figure of merit[c] (FOM) vs resolution									
d_{min}	total	7.62	4.91	3.87	3.30	2.92	2.64	2.44	2.27
N	54268	2848	4609	5817	6797	7600	8302	8901	9394
mean FOM	0.60	0.86	0.81	0.75	0.70	0.64	0.56	0.47	0.37

Final X-PLOR Model Refinement Summary

no. of protein molecules in the asymmetric unit	3
individual patatin molecular residue ranges[d]	
molecule 1	25−384
molecule 2	1024−1382
molecule 3	2022−2383
no. of water molecules	498
resolution (Å)	20−2.2
R_{work}[e] (90% of the data)	22.0
R_{free}[e] (10% of the data)	27.2
$\langle B\rangle$ (Å^2)	30.7
rms deviations from ideal geometry	
bonds (Å)	0.008
angles (deg)	1.272

[a] $R_{sym} = \sum|I_h - \langle I_h\rangle|/\sum I_h$, where $\langle I_h\rangle$ is the average intensity over symmetry equivalents. Numbers in parentheses represent statistics for the last shell. [b] Friedel pairs separate. [c] Figure of merit $= \langle|\sum P(\alpha)e^{i\alpha}/\sum P(\alpha)|\rangle$, where α is the phase and $P(\alpha)$ is the phase probability distribution. [d] Corresponding patatin residue numbers between molecules 1 and 2 and between molecules 2 and 3 differ in magnitude by 1000. [e] $R = \sum||F_{obs}| - |F_{calc}||/\sum|F_{obs}|$, where R_{free} is calculated for a randomly chosen 10% of the reflections and R_{work} is calculated for the remaining 90% of the reflections ($F > 2.0$) used for structure refinement.

and assayed for esterase activity. Fractions containing patatin were dialyzed against buffer A supplemented with 1 M ammonium sulfate and 1 mM β-mercaptoethanol. The protein was purified to homogeneity by loading it on a Phenyl-Sepharose 16/10 column (Amersham Pharmacia Biotech) equilibrated with the same and run with a 1 to 0 M ammonium sulfate reverse gradient at a flow rate of 3 mL/min. Patatin-containing fractions were pooled, concentrated, and dialyzed against buffer A. The purity of the proteins was analyzed by SDS−PAGE.

Steady-state kinetic assays at different pH values were performed using 50 mM MES for the pH range of 5−7.0, 50 mM TRIZMA for the pH range of 7−9.0, and 50 mM CHES for pH 9.5 in a total volume of 150 μL. Measurements were taken in triplicate. Enzyme activity could not be investigated below pH 5 because of enzyme instability. Assays were initiated with 10 μL of enzyme containing 0.1 mg/mL protein in 25 mM Tris-HCl (pH 7.5). The reactions were quenched after 5 min with 850 μL of 200 mM borate buffer (pH 9.8), and the absorbance was measured at 405 nm. The concentration of the reaction product, *p*-nitrophenol, was calculated using an extinction coefficient of 18 380 M^{-1} cm^{-1} (*39*). The steady-state kinetic data were analyzed using KINETASYST (IntelliKinetics).

Insect Bioassay. Assays for activity against larvae of *Diabrotica undecimpunctata howardi* (Southern corn rootworm) were carried out by overlaying a purified test sample on an agar diet similar to that described previously (*40*). Proteins to be tested were diluted in 25 mM Tris-HCl (pH 7.5) and overlayed on the diet surface at a final concentration of 100 or 200 ppm. Neonate larvae were allowed to feed on the diet. Mortality and growth stunting were evaluated after 6 days.

RESULTS

Data Collection, Phase Determination, Structure Solution, and Refinement. The crystallographic data collection, phase determination, and refinement statistics are presented in Table 1. The patatin Pat17 four-wavelength MAD data were essentially complete, highly redundant, and strong, with all wavelengths having an overall $\langle I/\sigma(I)\rangle$ of $\geq$33.2. The figure of merit versus resolution SOLVE phasing statistics for the 20−2.2 Å calculation are presented in Table 1. The 20−2.2 Å SOLVE calculation identified 34 Se sites, and the phases had an overall mean figure of merit (FOM) of 0.60; the 20−2.5 Å calculation identified 35 Se sites and had an overall mean FOM of 0.68. Comparing these two results using a solution comparison utility within the SOLVE program revealed that 32 sites were common. The high overall mean FOM values for the experimental phases obtained in these SOLVE calculations, coupled with the fact that the total number of Se sites identified was close to the maximum possible for three SeMet patatin molecules, 36, and the strong

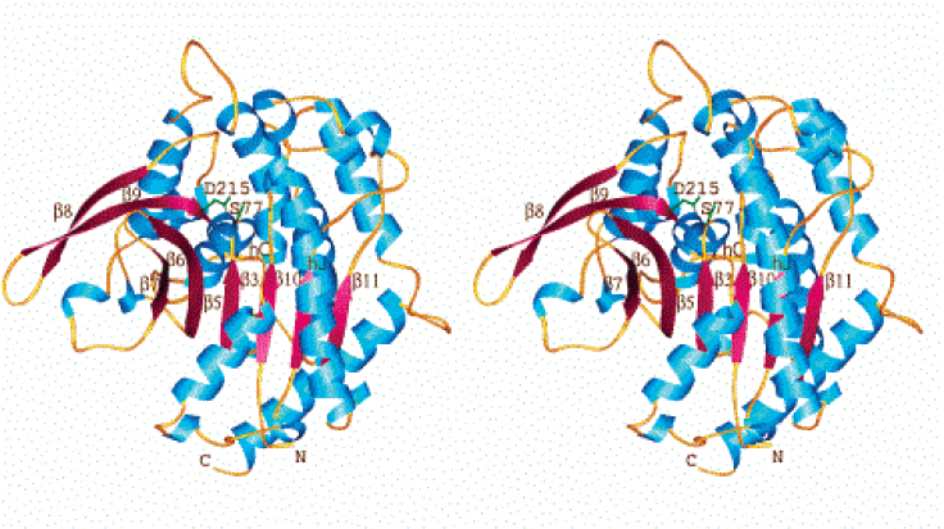

FIGURE 1: Stereo ribbon-style figure of the patatin Pat17 monomer. Helices are rendered in blue; β-strands are numbered (β3 and β5−β11) and rendered in maroon, and coil structure is rendered in gold. The catalytic dyad residues S77 and D215 are rendered in green. The N- and C-termini of the structure are indicated. This figure was prepared using Ribbons (*52*).

agreement between the two solutions, were early indications of the validity of the phases.

A 20−2.2 Å resolution electron density map calculated using the shortest wavelength data (λ_4 = 0.942 Å) and SOLVE-based phases modified using the CCP4 utility DM was of excellent quality. It was clear from the map that there were indeed three patatin Pat17 molecules in the asymmetric unit. Moreover, the high quality of the electron density along with the Se atom positions to mark the locations of the SeMet residues made tracing a single patatin molecule using the correct amino acid sequence proceed relatively smoothly. As mentioned previously, the patatin Pat17 construct used for crystallography had the 23-amino acid signal sequence replaced with the 10-amino acid hexahistidien tag sequence (MHHHHHHAMA). To maintain the original sequence numbering convention of the Pat17 gene, the first residue of the Pat17 crystallography protein sample was residue Met14. This initial map-built structure for patatin Pat17 contained sequence residues 27−384, lacking the first 13 residues at the N-terminus and the last three C-terminal residues. AmoRE molecular replacement using this coordinate set and 8−3.5 Å data readily located the remaining two molecules in the asymmetric unit, with a correlation coefficient of 60.8 and an *R*-factor of 38.4%.

A summary of the final patatin structure statistics after iterative map fitting and refinement is presented in Table 1. The final patatin structure contains three independent patatin Pat17 molecules and 498 water molecules. All three patatin molecules have similar though slightly different N- and C-termini. While the three Pat17 structures lack only two to four residues at the C-terminus, none possess an ordered N-terminal hexahistidine tag peptide region, which is not surprising since this nonnative sequence was added to aid purification. The structure has an R_{work} of 22.0% and an R_{free} of 27.2% for 20−2.2 Å data. Overall, the coordinates are of good geometry, with rms deviations from ideality of 0.008 Å in bond lengths and 1.272° in bond angles. Finally, PROCHECK Ramachandran plot analysis on the final coordinates indicates that the distributions of the residues in most favored, additionally allowed, and generously allowed regions are 88.3, 10.3, and 1.5%, respectively, with no residues in disallowed regions.

Molecular Structure of Patatin Pat17. The molecular structure of a patatin Pat17 monomer is displayed in Figure 1. The patatin monomer has dimensions of roughly 60 Å × 55 Å × 35 Å. Patatin displays an α/β class protein fold with approximately three layers, basically α/β/α in content, in which a central six-stranded β-sheet is sandwiched essentially between α-helices front and back. The central β-sheet contains five parallel strands and an antiparallel strand at the edge of the sheet. The three independent Pat17 patatin molecules in the asymmetric unit are related by a pseudo-3-fold axis, which is approximately oriented along the *c* axis of the crystal. The three molecules also have essentially the same structure. Pairwise root-mean-square differences in Cα positions among the three independent patatin molecules (residues 25−384, 1024−1382, and 2022−2382) over the common residue range of 25−382 vary from 0.19 to 0.23 Å. While the three patatin molecules are highly similar in structure, these unusually low values are due in part to the fact that the trimer was refined using NCS equivalent atom restraints that extended over ∼79% of the main chain atoms of each monomer.

Though the crystallographic asymmetric unit of patatin contains three molecules related by a pseudo-3-fold axis, there does not appear to be any biological significance to the trimer. Dynamic light scattering measurements conducted on a 20 mg/mL solution of patatin revealed a monodisperse sample consistent with patatin monomers in solution. In addition, solvent accessible surface calculations (SAS) conducted on the collective three-molecule patatin asymmetric unit and on each individual patatin monomer (Accelrys, Inc.) revealed that very little, 0.2% (100 Å^2 SAS out of 46 486 Å^2 SAS for the trimer), of the solvent accessible surface is buried in the patatin asymmetric unit. The pseudo-3-fold axis relating the patatin molecules in the asymmetric unit is simply a byproduct of the crystal packing. Finally, while this pseudo-3-fold axis approximately along the *c* axis of the crystal initially suggested that the patatin crystals might possess a trigonal or hexagonal lattice, careful indexing tests

revealed that the correct crystal lattice was C-centered orthorhombic.

Topology of the Patatin Fold. The structures of lipases from diverse origins, ranging from microbes to mammals, largely conform to the α/β-hydrolase fold (*21*). A Richardson diagram of the canonical α/β-hydrolase fold is displayed in Figure 2A. Defining features of this fold include a central eight-stranded β-sheet, in which the first two strands are antiparallel to one another and the remaining six strands are parallel, with the intervening helices occurring between the latter six strands sandwiching the central β-sheet. The catalytic serine residue is located in the sharp "nucleophile elbow" turn loop between strand β5 and helix C (*21*), and the remaining catalytic triad members, Asp/Glu and His, are located on other loops in the structure.

A Richardson diagram of the patatin Pat17 fold is displayed in Figure 2B. The secondary structural elements of patatin are designated on the basis of the α/β-hydrolase fold nomenclature outlined by Schrag and Cygler (*41*). The patatin fold comprises eight β-strands (β3 and β5−β11) and 12 α-helices (helices A−L), with a six-stranded central β-sheet. A comparison of panels A and B Figure 2 reveals some similarities between the patatin fold and the canonical α/β-hydrolase fold. The central core of the patatin fold is a mostly parallel β-sheet, like that of the canonical α/β-hydrolase fold. Also, the catalytic serine, Ser77, resides in a nucleophilic elbow loop following β5 and preceding helix C. An alignment of the Cα structure of patatin with a fungal lipase possessing the canonical α/β-hydrolase fold, *Rhizomucor miehei* lipase [PDB entry 3TGL (*42*)], highlights the structural similarity of the two enzymes in the vicinity of the nucleophilic serine. Thirty-four patatin Pat17 Cα atoms from strands β3 and β6, the contiguous peptide segment containing β5, the nucleophile elbow turn, and helix C align with 34 *R. miehei* lipase Cα atoms from strands β4 and β6 and the strand β5−nucleophile elbow−helix C segment with an an rms difference of only 1.1 Å. Thus, the structural elements surrounding the nucleophile in patatin are in a spatial arrangement similar to the arrangement of those found in the *R. miehei* lipase and likely other α/β-hydrolase fold enzymes.

Further analyses reveal that patatin is distinct from α/β-hydrolase fold enzymes in overall structure, topology, and connectivity. Though patatin and the *R. meihei* lipase share 34 spatially similar Cα atoms in the vicinity of the active site serine, much of the remaining protein structure is different between the two enzymes. A detailed comparison of the Richardson folding diagrams of the canonical α/β-hydrolase fold and of patatin clearly reveals that the patatin fold topology is distinct from that of the α/β-hydrolase fold. The central core of the patatin fold is a six-stranded sheet, while in the α/β-hydrolase fold, the central sheet is eight-stranded. In addition, the patatin central sheet contains five parallel β-strands followed by one antiparallel strand, while in the canonical α/β-hydrolase fold, there are two antiparallel β-strands followed by six parallel strands.

The patatin Pat17 fold topology displays some similarities with the fold topology of the catalytic domain of human cytosolic phospholipase A_2 ($cPLA_2$) (*17*), which is also a lipid acyl hydrolase with a Ser-Asp catalytic dyad. The Richardson drawing of the catalytic domain of $cPLA_2$ is displayed in Figure 2C. The $cPLA_2$ catalytic domain contains

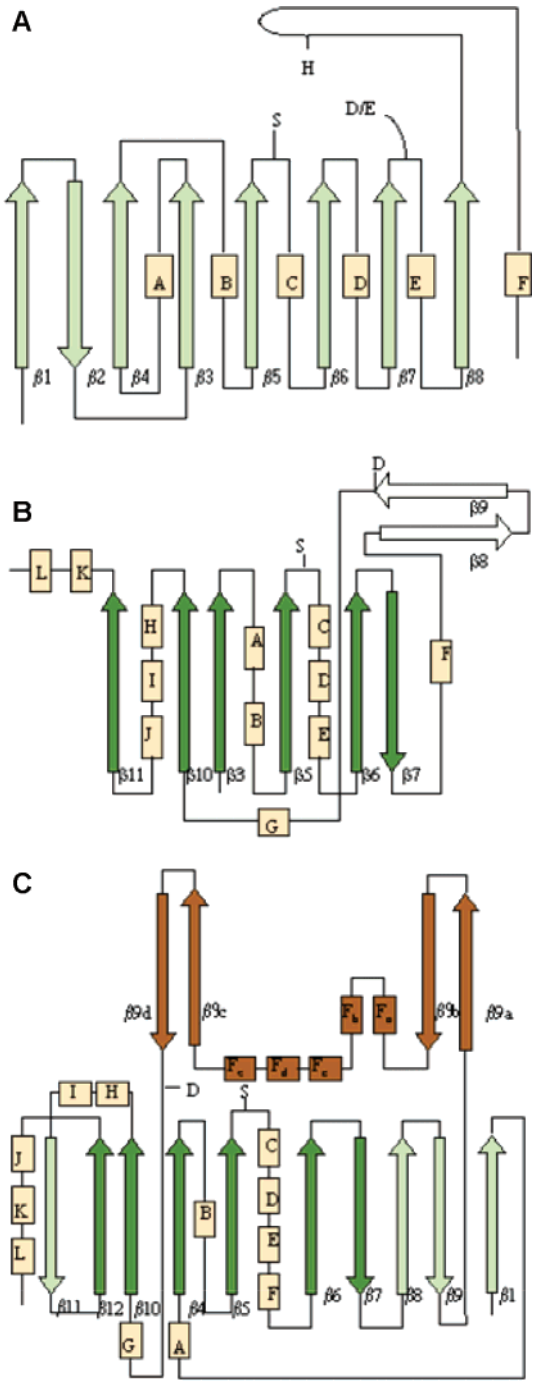

FIGURE 2: Richardson diagrams of the canonical α/β-hydrolase fold, patatin, and $cPLA_2$. (A) Richardson representation of the canonical α/β-hydrolase fold. β-Strands are represented as arrows, and helices are represented as rectangles. Secondary structural elements are designated on the basis of the review of Schrag and Cygler (*41*). The central core of the fold is the eight-stranded β-sheet, with the helices located on either side of the sheet. The catalytic triad residues are designated S, D/E, and H. (B) Richardson drawing of the patatin fold. The convention for naming secondary structural elements is that described for panel A. The six β-strands comprising the central β-sheet are colored dark green. The catalytic dyad residues are designated S and D. (C) Richardson drawing of the $cPLA_2$ fold. The convention for naming secondary structural elements is that described for panel A. The catalytic dyad residues are designated S and D. The central β-sheet of $cPLA_2$ contains 10 strands. The six strands of this sheet that correspond topologically with the six strands of the patatin central β-sheet are colored dark green. The secondary structural elements comprising the lid or cap of $cPLA_2$ are colored light brown.

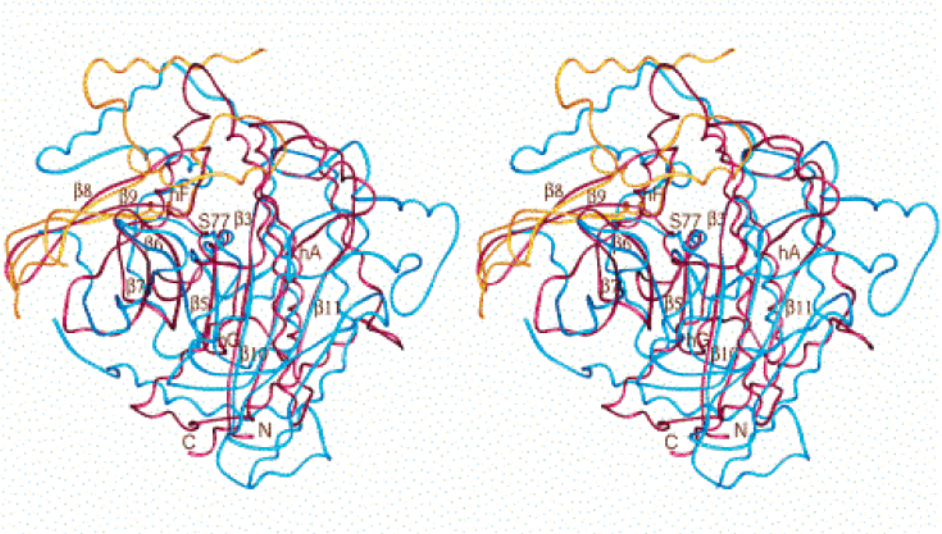

FIGURE 3: α-Carbon superposition of the $cPLA_2$ catalytic domain on patatin in stereo. This figure was prepared using Ribbons (*52*), and the view is the same as that in Figure 1. The alignment of patatin molecule 1 (residues 25−384) and the $cPLA_2$ catalytic domain (PDB entry 1CYJ, residues 144−721) was conducted using the program O utility 6d_lsqman. The patatin α-carbon trace is in maroon. The α-carbon trace of $cPLA_2$ residues (144−370 and 547−721) is rendered in cyan, while the α-carbon trace of the ordered lid or cap residues of $cPLA_2$ (370−432, 460−498, and 539−548) is rendered in gold. The root-mean-square difference in α-carbon positions using 111 corresponding residues is 2.06 Å. Most of the structural elements in patatin with corresponding features in $cPLA_2$ are noted in the figure, and include β-strands β3 and β5−β11 and helices hA, hF, and hG. The patatin N- and C-termini are also indicated.

a 10-stranded, mixed central β-sheet (β1 and β4−β12) with intervening helices, and a flexible lid region that is not part of the central core, which contains four β-strands (β9a−β9d) and five α-helices (Fa−Fe). Comparing panels B and C of Figure 2 reveals that patatin and $cPLA_2$ both possess a central, mixed β-sheet with intervening helices, a catalytic serine in the nucleophilic elbow turn following β5 and preceding helix C, and a catalytic Asp preceding helix G. An optimal Cα structural alignment performed using molecule 1 of patatin and the $cPLA_2$ catalytic domain reveals that there is a significant amount of spatial and topological similarity between the two enzymes; the results of this alignment are presented in Figure 3. All six of the β-strands which comprise the central β-sheet of patatin (β3, β5−β7, β10, and β11) and three α-helices (A, C, and G) superimpose well with structural elements within the $cPLA_2$ catalytic domain. Because the central β-sheet of patatin is contained within the central β-sheet of $cPLA_2$ and because both enzymes contain helices interspersed between the β-strands, one might conclude that the patatin fold topology is related to that of $cPLA_2$.

Patatin Active Site. The patatin Pat17 crystal structure (Figure 1) clearly revealed what was suggested by our own mutational, enzyme activity, and bioassay studies and the structure−function studies of others (*16*), that a hallmark feature of its active site is the Ser-Asp catalytic dyad, as opposed to a Ser-, Asp-, and His-containing catalytic triad, which is typical of lipid acyl hydrolases (*21*). These active site residues are actually located in a binding channel, which is visible from the molecular surface rendition of patatin displayed in Figure 4.

A detailed stereoview of the patatin active site region within the binding channel is displayed in Figure 5. The curved "back wall" of the active site binding channel contains, from left to right in Figure 5, the catalytic aspartate, Asp215, and the catalytic serine, Ser77, residues, as well as Gly37, Gly38, and Arg40. What is noteworthy about all of this is that these residues are important to and in essentially the same spatial location as in the active site region of the catalytic domain of $cPLA_2$ (*17*). Both the patatin and $cPLA_2$ enzymes contain a catalytic serine in a turn between strand β5 and helix C (Figure 2B,C): Ser77 in patatin and Ser228 in $cPLA_2$. Like other lipid acyl hydrolases and α/β-hydrolase fold enzymes, patatin's catalytic Ser77 residue lies in a Gly-X-Ser-X-Gly sequence motif and in a nucleophilic elbow loop following strand β5 and preceding helix C (*43*). The catalytic Ser228 of $cPLA_2$ also lies in a loop following strand β5 and preceding helix C, but it lies in a Gly-X-Ser-Gly-

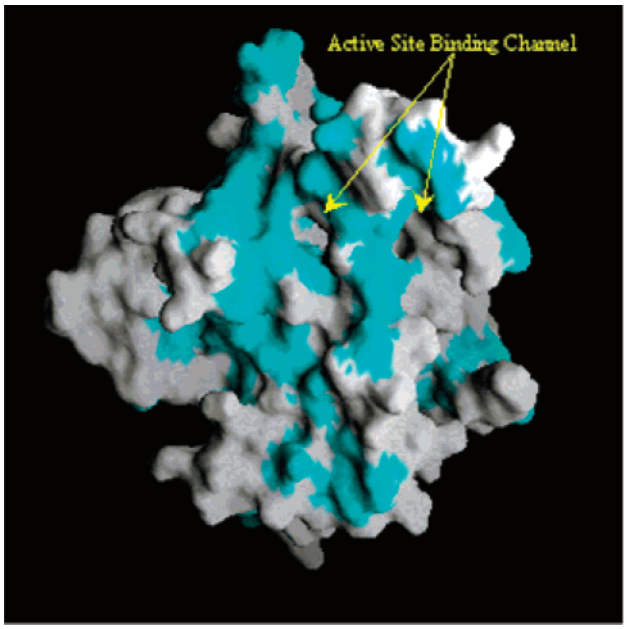

FIGURE 4: Molecular surface views of patatin with hydrophobic surface residues highlighted. Exposed surfaces of all hydrophobic residues have been colored blue. This figure was prepared with GRASP (*53*). The view is the same as the orientation in Figure 1. The two entry−exit points which define patatin's active site binding channel are indicated.

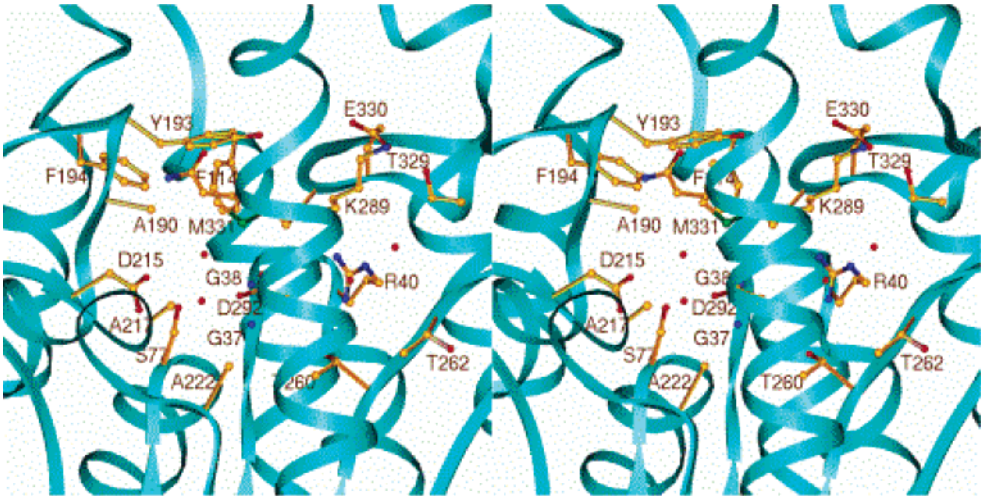

FIGURE 5: Stereo ribbon-style figure of the patatin active site binding channel. This figure was prepared using Ribbons (*52*). Molecule 2 of the patatin asymmetric unit was used to prepare the figure. For simplicity, the residues are numbered as for molecule 1. The protein backbone is rendered as a cyan ribbon, and selected residue carbon, nitrogen, and oxygen atoms are rendered in gold, red, and violet, respectively. Four water molecules in the channel are rendered as red oxygen atoms.

Ser sequence motif. Both enzymes contain a catalytic aspartic acid residue, Asp215 in patatin and Asp549 in cPLA$_2$, at or near the terminus of the last β-strand segment outside the central β-sheet defining the core structure, strand β9 in patatin and strand β9d in cPLA$_2$. In addition, both enzymes contain a Gly-Gly-X-Arg sequence motif that is important in defining the oxyanion hole of the active site; in patatin, this sequence is Gly37-Gly38-X-Arg40, and in cPLA$_2$, this sequence is Gly197-Gly198-X-Arg200 (*17*). The nitrogen atoms of the two successive glycine residues define the oxyanion hole, and stabilize the oxyanion that forms during the nucleophilic attack by the catalytic serine during substrate cleavage. Finally, the arginine residues of both enzyme active sites have side chain guanidinium group orientations that could stabilize the phosphate moiety of a phospholipid substrate (*17*). All in all, the structural similarity of the patatin active site to that of cPLA$_2$ suggests that the catalytic mechanisms governing the functioning of both Ser-Asp lipid acyl hydrolases are likely similar (*17*).

Figure 5 also displays the patatin Pat17 residues that are important in defining the "floor", "ceiling", and "front wall" of the active site binding channel, which appears to be the entryway for substrate catalysis. The floor of the binding channel is defined by residues Ala217, Ala222, Thr260, and Thr262. The front wall of the binding channel is defined by selected residues from helix J, with the Asp292 side chain pointing into the channel. The ceiling of the binding channel, moving from left to right in Figure 5, is defined by the side chains of residues Ala190, Phe194, Tyr193, Gln288, Phe114, Met331, Lys289, Glu330, and Thr329.

The active site region and overall structure of patatin B2, the patatin enzyme that was the focus of a recent publication by Hirschberg et al. (*16*), will be highly similar to those of Pat17, since the sequences of these two patatins are 87% identical over the common 364 residues beyond the N-terminal signal sequence region. The Hirschberg et al. paper reveals that the patatin B2 active site region contains serine (Ser54), aspartate (Asp192), and glycine residues (Gly14 and Gly15) (*16*) analogous to the active site-defining residues of patatin Pat17. The patatin B2 active site differs slightly from that of Pat17 in that it contains a homologous Lys residue, Lys17, near the oxyanion hole-defining Gly residues rather than an arginine (*16*). All other isozymes of patatin contain a Lys residue rather than an Arg at this position. By extension from the cPLA$_2$ structure, a possible role for the Pat17 Arg40 residue guanidinium group is to interact with the phosphate moiety of a substrate; a Lys ammonium group could also stabilize the phosphate moiety of a suitable phospholipid substrate bound in the active site.

Comparison of the Sequences of Pat17 and Other Patatin Isozymes. Sequence analysis indicates that Ser77 in Pat17 lies in the conserved amino acid motif (Gly-X-Ser-X-Gly) describing esterases (*4*−*6*, *15*). In addition, a sequence comparison of Pat17 with other patatin sequences obtained from GenBank identified numerous patatins (for example, GenBank entries S51596, P15478, P11768, T07592, B26017, P07745, P15477, AAA33828, and A24142) with a high level of sequence conservation around the oxyanion hole glycine residues (Gly37 and Gly38), the catalytic serine (Ser77), and the catalytic aspartate (Asp215).

Esterase Activity. Table 2 shows the list of charged to alanine scan variants. All the variants were expressed in *P. pastoris* and assayed for esterase activity as shown in Table 2. The level of protein expression in the culture supernatants was assayed using an ELISA, and Western blots were utilized to confirm that the electrophoretic mobility was equivalent to that of wild-type Pat17. Some of the variants could not be detected using both ELISA and immunoblotting analysis, such as variants E52A, D68A, D71A, R94A, E108A, H109A, E149A, D156A, K167A, D177A, D300A, and R318A. The variant D215A showed no detectable esterase activity but was expressed in normal amounts and was readily detected by immunoblot analysis and an ELISA, suggesting that this residue is critical for esterase activity. As Ser77 lies in the hydrolase motif, we also made a S77A variant to elucidate its role in catalysis. S77A showed no detectable esterase activity but was expressed in normal amounts as assessed by immunoblot analysis and an ELISA, suggesting that this residue is necessary for catalysis. Several variants were then made at position 77, including S77D, S77T, S77N, S77C, and S77R, to elucidate the primary sequence requirements for enzymatic activity. The variants at positions 77 and 215

Table 2: Charged to Alanine Scan Variants[a]

	normalized activity (*p*-nitrophenyl octanoate/ *p*-nitrophenyl caprate)		normalized activity (*p*-nitrophenyl octanoate/ *p*-nitrophenyl caprate)
wild type	1.0	K251A/K252A	1.3
E27A	0.7	E265A/D267A	0.5
D35A	0.5	K268A	0.9
R40A	1.0	K273A	1.0
E49A	1.1	E274A	0.9
E57A/D59A	1.9	H282A	0.7
D63A	0.7	K289A	0.6
R65A	0.6	D292A	0.4
E91A	1.0	D311A	0.4
K100A	0.9	K313A	0.7
E101A	1.0	E321A	1.1
K124A	0.5	E330A	0.5
D126A	0.6	D332A	0.7
K128A	0.7	D333A	0.4
E136A	0.8	E336A	0.5
K137A	0.9	E340A	0.6
E140A	1.6	E347A	0.8
R142A	0.6	K351A/K352A	0.8
H144A	0.6	E356A/D357A	0.5
K158A	0.8	E360A	0.6
K161A	0.6	E363A	0.5
E175A	1.0	E364A	0.5
K179A	0.5	K367A	0.4
D182A	0.3	R368A	1.0
H197A	0.7	K371A	0.7
D207A/E208A/E210A	0.8	D375A	0.6
D223A	1.2	R376A	0.6
R234A	0.7	K377A	0.5
K238A	0.8	K378A	0.6
D239A	0.6	R380A	0.5
R246A	0.4	K383A	0.5

[a] The average error associated with these measurements was 22%.

were purified to homogeneity and assessed for esterase activity. The results of the esterase activity assay for the purified variants at positions 77 and 215 are shown in Table 3. All the Ser77 variants were found to have 0.1−0.01% esterase activity with no detectable expression of the S77R variant. The D215A variant had 0.02% activity compared to the wild-type enzyme. These results suggest that Ser77 and Asp215 are residues involved in catalysis. Esterase activity of all the other variants varied from 1.9- to 0.3-fold of that of the wild-type protein (Table 2). Histidine is a conserved residue in the normal lipase catalytic triad (*15*), and in the "charged to alanine" scan variants, we observed that three of the four His residues (H144A, H197A, and H282A) maintained full enzymatic activity (Table 2). One His variant, H109A, could not be expressed. A variant with an isosteric substitution of His to Asn at position 109, H109N, maintained full enzymatic activity. Other changes at this position, including H109C and H109R, could not be obtained in sufficient quantities in *P. pastoris*, suggesting that His109 or an isosteric substitution with Asn is critical for maintaining the stability of the enzyme. This result also indicates that His109 does not play a direct role in catalysis.

Ser77, His109, and Asp215 are conserved within the known patatin enzymes, confirming the importance of these residues in the function of patatins. In fact, these residues lie within regions of near-total conservation among the nine patatin sequences that were examined.

pH Dependence of Kinetic Parameters. The pH dependence of kinetic parameters k_{cat}/K_m of *p*-nitrophenyl caprate hydrolysis was used to determine the states of protonation of groups on the enzyme that affect catalysis and/or substrate binding (*44*). The kinetic parameters were obtained by varying *p*-nitrophenyl caprate as described in Experimental Procedures, and the data were analyzed using KINETASYST (IntelliKinetics). The kinetics data at different pH values were then plotted as the log of k_{cat}/K_m versus pH and are shown in Figure 6. The pH-independent value of the kinetic parameters are as follows: $k_{cat} = 2.8 \pm 0.2$ s^{-1} and $K_m = 0.26 \pm 0.04$ mM. k_{cat}/K_m is essentially pH-independent over the pH range of 5−9.5. The profile clearly presents no evidence of titratable groups such as a histidine being involved in catalysis over the pH range that was studied. These data are consistent with a single residue having a pK_a of <5 being deprotonated during catalysis, which in this case is Asp215. Furthermore, these data are in agreement with the alanine-scanning mutagenesis and X-ray structural analysis results that support a Ser-Asp catalytic dyad in patatin.

Insect Bioassay. Since it has previously been shown that the enzymatic activity of patatin is correlated with bioactivity (*9*), we assayed all of the purified variants, including S77A, S77D, S77T, S77N, S77C, and D215A, against Southern corn rootworm (SCRW). All of the assays were performed by overlaying protein (final concentration of 200 ppm) on diet as explained in Experimental Procedures. The results are shown in Figure 7. The wild-type protein caused significant stunting of the larval growth as measured by the weight of the larvae. All the esterase inactive variants had no activity against SCRW, suggesting that Ser77 and Asp215 are necessary for insecticidal activity in addition to esterase activity. Assays were also conducted to evaluate the bio-

Table 3: Esterase Activity of Purified Variants at Positions 77, 109, and 215

	esterase activity (ΔOD min^{-1} μg^{-1})		esterase activity (ΔOD min^{-1} μg^{-1})
wild type	116.0	S77N	0.01
S77A	0.02	S77C	0.1
S77D	0.01	H109N	234.5
S77T	0.1	D215A	0.02

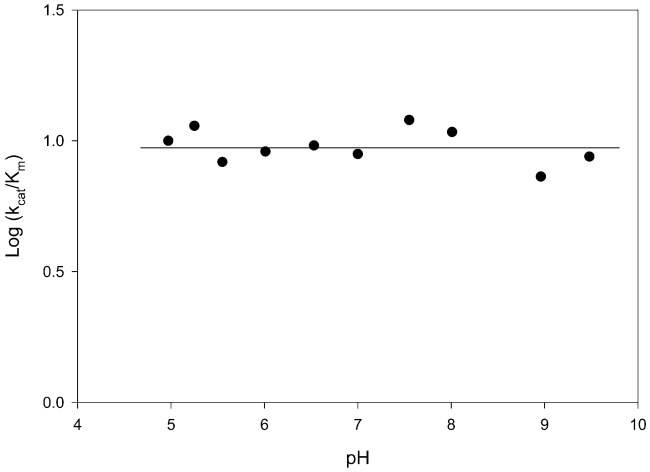

FIGURE 6: pH−rate profile. The data were not fit to any equation.

activity of the H109N variant in a manner similar to that used for the other variants. As shown in Figure 8, H109N had activity similar to that of the wild-type enzyme in inhibiting the growth of SCRW larvae.

DISCUSSION

Determining the X-ray crystal structure of patatin Pat17 to 2.2 Å resolution confirmed that indeed its active site contains a Ser-Asp catalytic dyad, and that the active site region is very similar to that observed in another lipid acyl hydrolase with a Ser-Asp catalytic dyad, human cPLA$_2$ (*17*). The patatin crystal structure reveals that the catalytic serine displays structural characteristics like those observed in other α/β-hydrolase fold enzymes, most notably, that it resides in a sharp nucleophile elbow turn loop which follows a β-strand (β5) of the central β-sheet and precedes a helix (helix C) (*21*). However, the folding topology of patatin is significantly different from that of the consensus α/β-hydrolase fold (*21*), and is more closely related to that observed for human cPLA$_2$ (*17*).

The patatin crystal structure also validates biochemical and mutational data obtained by us and by others for the enzyme. The Pat17 structure reveals that Ser77 is the catalytic serine in the Ser-Asp active site dyad. As expected, Ser77 resides in the general amino acid sequence motif characteristic of the active site serine residues in serine hydrolases, Gly-X-Ser-X-Gly (*4*−*6*, *9*, *15*). This was confirmed by our Ser77 mutational work, which involved mutating this residue to Ala, Asp, Thr, Asn, or Cys. Enzyme activity studies of the variants showed that substitution of Ser77 essentially abolished the esterase activity (Table 3). Our Southern corn rootworm bioactivity assays of these Ser77 variants also revealed that the catalytic serine was critical to insecticidal activity as well (Figure 7), something that had been suggested previously by Strickland et al. with DFP-treated patatin (*9*).

The crystal structure determination of Pat17 clearly revealed that the catalytic aspartate residue in the active site dyad was Asp215. This was consistent with our mutagenesis studies that identified Asp215 as the carboxylate residue that was critical for enzymatic activity (Table 3). In addition, our pH−rate profile data on Pat17 revealed no ionizable group, such as imidazole, with a pK_a from 5 to 9.5 was essential for activity (Figure 6). However, this behavior could certainly be explained by the involvement of an aspartate residue such as Asp215, which has an ionizable carboxylate proton with a pK_a of <5. A comparison of the Pat17 sequence with other patatins indicated that Ser77 and Asp215 of Pat17 were conserved in all the patatins that were examined, suggesting that these residues perform a critical role; clearly, our structural, mutational, enzymatic, and bioactivity studies with Pat17 help one understand why this is the case.

Patatin is classified as a lipid acyl hydrolase because it exhibits phospholipase activity (*9*, *11*). Lipid acyl hydrolases frequently contain catalytic triads consisting of Ser, Asp or Glu, and His residues (*15*). Our Pat17 crystal structure along with our mutational and activity studies clearly revealed that there is no key His residue in the enzyme active site, or one that is absolutely critical to the enzymatic activity or bioactivity of Pat17. However, these same studies helped us understand why one His residue, His109, appears to be important to enzymatic stability. Substitution of Ala, Cys, or Arg at position 109 was not permitted, as no protein could be detected with an ELISA and immunoblotting, suggesting that this position might be crucial for the stability of the enzyme. Yet, a H109N change at this position generates a protein that maintains full esterase and insecticidal activity (Table 3 and Figure 8). The esterase activity of H109N was increased by 2-fold but exhibited insecticidal activity similar to that of the wild-type enzyme. It has been shown previously that there is no direct correlation between esterase activity and insect larval growth inhibition (*9*). Examining the Pat17 crystal structure in the vicinity of His109 and modeling a H109N mutation provided some insights into why this substitution is likely tolerated. In Pat17, a His109 side chain nitrogen atom participates in a hydrogen-bonded interaction with the side chain hydroxyl group of Tyr129 (2.8 Å). This hydrogen bond appears to be important to the stabilization of the helix D−turn−helix E structural motif in the enzyme. When this His residue was replaced with an Asn by molecular modeling, this neutral, nearly isosteric mutation resulted in the maintenance of a structurally similar hydrogen bonding interaction (2.9 Å), maintenance of a helix D−turn−helix E motif stabilizing interaction, and thus a stable variant. Ala, Cys, or Arg mutations at position 109 are not isostructural substitutions, would not maintain the hydrogen bond interaction with Tyr129, and would likely disrupt the helix D−turn−helix E structure of the enzyme; for these reasons, these mutations are destabilizing. Sequence comparison of patatins in the His109 region of Pat17 indicated that His109 was conserved across all the patatins that were examined, suggesting that a His residue at this position plays a critical role in the stability of the enzyme.

The Pat17 crystal structure also provided insights into why patatin does not exhibit interfacial activation (*23*, *24*), a characteristic feature of lipases, and why it is active on lipids in solution rather than at an oil−water interface. Interfacial activation is a phenomenon displayed by lipases in which

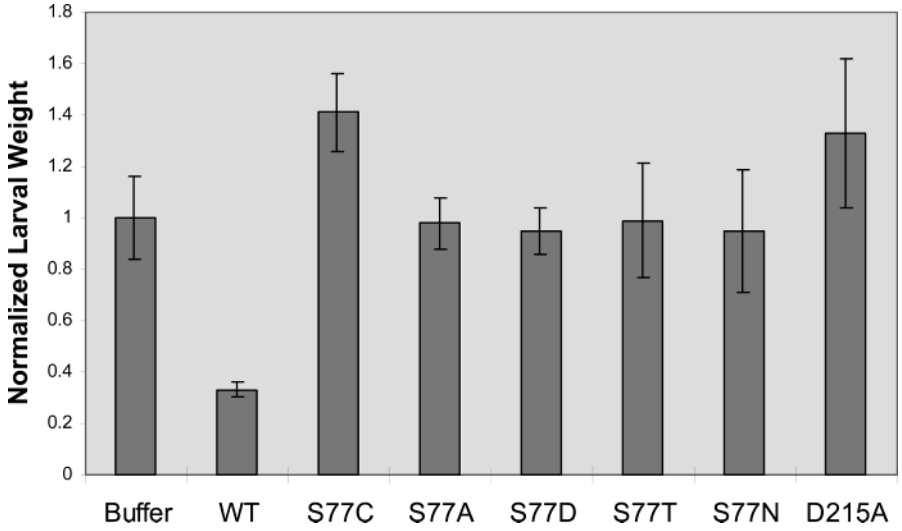

FIGURE 7: Effect of Pat17 and variants on growth of neonate SCRW larvae. The protein was overlayed on diet at a final concentration of 200 ppm. The assay consisted of 16 replicates per sample.

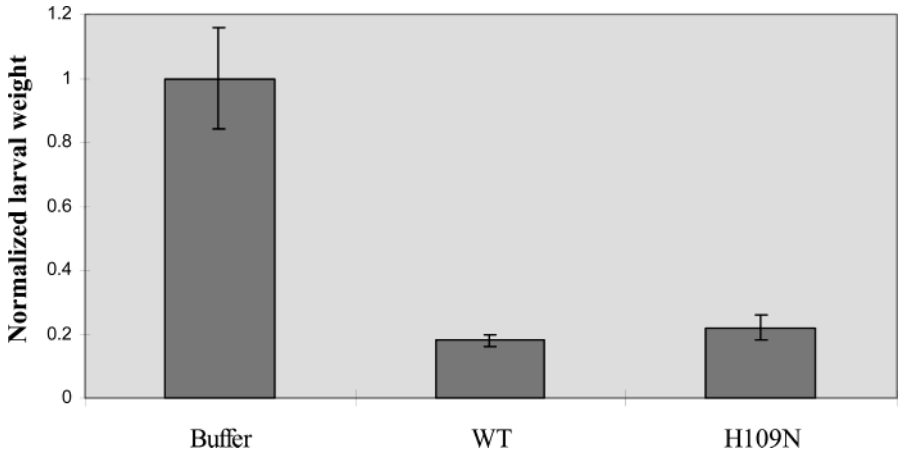

FIGURE 8: Effect of the wild type and H109N variant on the growth of neonate SCRW larvae. The protein was overlayed on diet at a final concentration of 100 ppm. The assay consisted of 16 replicates per sample.

the catalytic activity of the enzyme is greater when a substrate is in a micelle than in solution. A common explanation for this behavior is that lipases possess a flexible "lid" that regulates access to the hydrophobic, active site region (*41*). Crystal structures of a number of lipases have revealed that the lids contain at least one amphipathic α-helix, and that the underside of the lid contains predominantly hydrophobic residues while the portion facing the surface contains predominantly hydrophilic amino acids (*45*). Lipase crystals grown in the presence of substrate analogues or under hydrophilic solution conditions favor a "closed lid" conformation, while lipase crystals grown under low-polarity conditions favor "open lid" conformations (*41*, *45*, *46*). By analogy, in hydrophilic solution environments, the lipase lid would favor a closed conformation, and when this conformation is predominant, the rate of substrate catalysis is low, as access to the active site is poor. Moreover, in hydrophobic solution environments, such as when a lipase encounters a membrane or micellar lipid surface, substrate catalysis is significantly enhanced. In this environment, it is energetically favorable for the protein hydrophobic surface under the lid to interact with the micellar surface, and having the lid in the open conformation results in more active site access and therefore more substrate hydrolysis.

The human $cPLA_2$ enzyme is interfacially activated (*47*), and this is likely related to the fact that it contains a sizable lid structure, colored brown in Figure 2B and gold in Figure 3, which occludes access to the hydrophobic surface in the vicinity of its active site funnel (*17*), and which would favor the open conformation in a hydrophobic, micellar environment. Patatin, in contrast, does not exhibit interfacial activation (*9*, *24*). This observation is now consistent with the structure, since the Pat17 enzyme appears to possess no lid-like structural element for modulation of access to its active site binding channel (Figures 1 and 4). Figure 4 displays the molecular surface of patatin on the face containing the active site binding channel. The figure reveals that the molecular surface around the binding channel is largely hydrophobic in character. As the Pat17 patatin crystals were grown under hydrophilic solution conditions, using PEG 3350, Tris buffer, and ammonium acetate, one would expect that if the enzyme had a lid structure, it would likely adopt a closed conformation in this crystal structure to bury or shield the hydrophobic protein surface near the binding channel. However, because there is no such structural element in patatin, access to the substrate binding channel is unrestricted. It is noteworthy that patatin does possess an antiparallel loop structural element, directed away from the

active site binding channel, containing strands β8 and β9 (Figures 1, 2B, and 3) which is topologically in the same relative position as the lid structure extending from strand β9a to β9d in $cPLA_2$ (Figures 2C and 3). One therefore might expect that if patatin did have a lid, it would manifest itself by having amphipathic helical structures and more sheet structures in this region of the sequence.

Because patatin is not an interfacially activated lipase-like enzyme, it cannot hydrolyze lipids in a micellar environment. Yet, it is thought that the insecticidal activity may stem from the fact that patatin is indirectly responsible for disruption of insect midgut membranes (*9*). Strickland et al. (*9*) noted that patatin may act on solubilized lipids released during plant tissue disruption or digestion. This produces free fatty acids and partially hydrolyzed lipid species that can further disrupt membranes and solubilize more lipids, inducing an "autocatalytic" degradation of membranes (*24*). This autocatalytic membrane disrupting activity by patatin is believed to explain why membranes and lipids undergo rapid deterioration when potato tissue is damaged (*24*).

In conclusion, all of our data reveal that patatin is a lipid acyl hydrolase with a Ser-Asp catalytic dyad similar to that observed in the catalytic domain of human $cPLA_2$. Catalytic dyads have been observed previously in certain serine proteases, including those that use hydroxyl/ϵ-amine or hydroxyl/α-amine catalytic dyads to perform catalysis (*48*−*51*). The identification of a new class of lipid acyl hydrolases that utilize Ser-Asp catalytic dyads, which includes patatins and $cPLA_2$, suggests that other "dyad" variations on the classical catalytic triad theme, in addition to the Ser/Asp and Ser/Lys dyads, may yet exist. Further structure−function studies of these and other catalytic dyad-containing enzymes will lead to a better understanding of these intriguing molecules.

ACKNOWLEDGMENT

We thank Ravi Kurumbail, Jennifer Pawlitz, and Anna Stevens for their early technical involvement in the crystallographic work on patatin. The SeMet multiwavelength anomalous dispersion diffraction data used to determine the crystal structure of Pat17 patatin were collected at beamline 17-ID in the facilities of the Industrial Macromolecular Crystallography Association Collaborative Access Team (IMCA-CAT) at the Advanced Photon Source. The technical assistance of Jim Kiefer during this data collection was helpful. Use of the Advanced Photon Source was supported by the U.S. Department of Energy, Basic Energy Sciences, Office of Science, under Contract W-31-109-Eng-38. These IMCA-CAT facilities are supported by the companies of the Industrial Macromolecular Crystallography Association through a contract with the Illinois Institute of Technology (IIT), and executed through the IIT Center for Synchrotron Radiation Research and Instrumentation. We thank Richard Thoma for doing mass spectral analyses on our SeMet patatin sample and Eric Sturman for preparing the Richardson figures. We thank Leigh English, Ken Gruys, Ravi Kurumbail, Doug Sammons, and Jeff Seale for critical reading of the manuscript. Finally, we appreciated the continual support of Leigh English and Ken Gruys over the course of this work.

REFERENCES

1. Ganal, M. W., Roeder, M., Park, W., and Tanksley, S. (1991) *Mol. Gen. Genet. 225*, 501−509.
2. Vancanneyt, G., Sonnewald, U., Hofgen, R., and Willmitzer, L. (1989) *Plant Cell 1*, 533−540.
3. Hofgen, R., and Willmitzer, L. (1990) *Plant Sci. 66*, 221−230.
4. Mignery, G. A., Pikaard, C. S., Hannapel, D. J., and Park, W. D. (1984) *Nucleic Acids Res. 12*, 7987−8000.
5. Mignery, G. A., Pikaard, C. S., and Park, W. D. (1988) *Gene 62*, 27−44.
6. Stiekema, W. J., Keidekamp, F., Dirske, W. G., van Beckum, J., de Haan, P., ten Bosch, C., and Louwerse, J. D. (1988) *Plant Mol. Biol. 11*, 255−269.
7. Hirayama, O., Matsuda, H., Takeda, H., Maenaka, K., and Takatsuka, H. (1975) *Biochim. Biophys. Acta 384*, 127−137.
8. Wardale, D. A. (1980) *Phytochemistry 19*, 173−177.
9. Strickland, J., Orr, G., and Walsh, T. (1995) *Plant Physiol. 109*, 667−674.
10. Rosahl, S., Schmidt, R., Schell, J., and Willmitzer, L. (1986) *Mol. Gen. Genet. 203*, 214−220.
11. Senda, K., Yoshioka, H., Doke, N., and Kawakita, K. (1996) *Plant Cell Physiol. 37*, 347−353.
12. Park, W. D., Blackwood, C., Mignery, G. A., Hermodson, M. A., and Lister, R. M. (1983) *Plant Physiol. 71*, 156−160.
13. Sonnewald, U., Sturm, A., Chrispeels, M. J., and Willmitzer, L. (1989) *Planta 179*, 171−180.
14. Sonnewald, U., Schaewen, A. V., and Willmitzer, L. (1990) *Plant Cell 2*, 345−355.
15. Schrag, J. D., Li, Y., Wu, S., and Cygler, M. (1991) *Nature 351*, 761−764.
16. Hirschberg, H. J. H. B., Simons, J.-W. F. A., Dekkar, N., and Egmond, M. R. (2001) *Eur. J. Biochem. 268*, 5037−5044.
17. Dessen, A., Tang, J., Schmidt, H., Stahl, M., Clark, J., Seehra, J., and Somers, W. (1999) *Cell 97*, 349−360.
18. Cunningham, B., and Wells, J. (1989) *Science 244*, 1081−1085.
19. Bennett, W. F., Paoni, N. F., Keyt, B. A., Botstein, D., Jones, A. J. S., Presta, L., Wurm, F. M., and Zoller, M. J. (1991) *J. Biol. Chem. 266*, 5191−5201.
20. Hendrickson, W. A., Horton, J. R., and LeMaster, D. M. (1990) *EMBO J. 9*, 1665−1672.
21. Ollis, D. L., Cheah, E., Cygler, M., Dijkstra, B., Frolow, F., Franken, S. M., Harel, M., Remington, S. J., Silman, I., Schrag, J., Sussman, J. L., Verschueren, K. H. G., and Goldman, A. (1992) *Protein Eng. 5*, 197−211.
22. Desnuelle, P. (1972) in *The Enzymes* (Boyer, P. D., Ed.) pp 575−616, Academic Press, New York.
23. Verger, R. (1980) *Methods Enzymol. 64*, 340−392.
24. Galliard, T. (1980) in *The Biochemistry of Plants* (Stumpf, P. K., and Conn, E. E., Eds.) pp 85−116, Academic Press, New York.
25. Doublie, S., and Carter, C. W., Jr. (1992) in *Crystallization of Nucleic Acids and Proteins. A Practical Approach* (Ducruix, A., and Geige, R., Eds.) pp 311−317, Oxford University Press, New York.
26. Harp, J. M., Timm, D. E., and Bunick, G. J. (1998) *Acta Crystallogr. D54*, 622−628.
27. Matthews, B. W. (1968) *J. Mol. Biol. 33*, 491−497.
28. Rossmann, M. G. (1972) *The Molecular Replacement Method*, Gordon & Breach, New York.
29. Otwinowski, Z., and Minor, W. (1997) in *Methods in Enzymology: Macromolecular Crystallography, Part A* (Carter, C. W., Jr., and Sweet, R. M., Eds.) pp 307−326, Academic Press, New York.
30. Terwilliger, T. C., and Berendzen, J. (1999) *Acta Crystallogr. D55*, 849−861.
31. Project, C. C. (1994) *Acta Crystallogr. D50*, 760−767.
32. Jones, T. A., Zou, J. Y., Cowan, S. W., and Kjeldegaard, M. (1991) *Acta Crystallogr. A47*, 110−119.
33. Navaza, J. (1994) *Acta Crystallogr. A50*, 157−163.
34. Brunger, A. T. (1992) *X-PLOR: A system for X-ray crystallography and NMR*, Yale University Press, New Haven, CT.
35. Brunger, A. T. (1992) *Nature 355*, 472−474.
36. Adams, P. D., Pannu, N. S., Read, R. J., and Brunger, A. T. (1997) *Proc. Natl. Acad. Sci. U.S.A. 94*, 5018−5023.
37. Laskowski, R. A., MacArthur, M. W., Moss, D. S., and Thornton, J. M. (1993) *J. Appl. Crystallogr. 26*, 283−291.
38. Kunkel, D. A. (1985) *Proc. Natl. Acad. Sci. U.S.A. 82*, 477−492.
39. Bowers, G. N., McComb, R. B., Christensen, R. G., and Schaffer, R. (1980) *Clin. Chem. 26*, 724−729.

40. Marrone, P. G., Ferri, F. D., Mosley, T. R., and Meinke, L. J. (1985) *J. Econ. Entomol. 78*, 290−293.
41. Schrag, J. D., and Cygler, M. (1997) *Methods Enzymol. 284*, 85−107.
42. Derewenda, Z. S., Derewenda, U., and Dodson, G. G. (1992) *J. Mol. Biol. 227*, 818.
43. Derewenda, Z. S., and Derewenda, U. (1991) *Biochem. Cell Biol. 69*, 842−851.
44. Colanduoni, J., Nissan, R., and Villafranca, J. J. (1987) *J. Biol. Chem. 262*, 3037−3043.
45. Rubin, B. (1994) *Struct. Biol. 1*, 568−572.
46. Schrag, J. D., Li, Y., Cygler, M., Lang, D., Burgdorf, T., Hect, H.-J., Schmid, R., Schomberg, D., Rydel, T. J., Oliver, J. D., Strickland, L. C., Dunaway, C. M., Larson, S. B., Day, J., and McPherson, A. (1997) *Structure 5*, 187−202.
47. Nalefski, E. A., Sultzman, L. A., Martin, D. M., Kriz, R. W., Towler, P. S., Knof, J. L., and Clark, J. D. (1994) *J. Biol. Chem. 269*, 18239−18249.
48. Paetzel, M., and Strynadka, N. (1999) *Protein Sci. 8*, 2533−2536.
49. Paetzel, M., and Dalbey, R. (1997) *Trends Biochem. Sci. 22*, 28−31.
50. Slilaty, S., and Little, J. (1987) *Proc. Natl. Acad. Sci. U.S.A. 84*, 3987−3991.
51. Tschantz, W., Sung, M., Delgado-Partin, V., and Dalbey, R. (1993) *J. Biol. Chem. 268*, 27349−27354.
52. Carson, M. (1991) *J. Appl. Crystallogr. 24*, 958−961.
53. Nicholls, A., Sharp, K. A., and Honig, B. (1991) *Proteins 11*, 282−296.

BI027156R